Enhanced second-harmonic generation in coupled microcavities based on all-silicon photonic crystals

D. G. Gusev, I. V. Soboleva, M. G. Martemyanov, T. V. Dolgova, A. A. Fedyanin, and O. A. Aktsipetrov*
Department of Physics, Moscow State University, 119992 Moscow, Russia
(Received 5 July 2003; revised manuscript received 29 September 2003; published 8 December 2003)

The enhancement of second-harmonic generation (SHG) in one-dimensional coupled photonic-crystal microcavities (CMC) formed from mesoporous silicon is observed. Peaks in the angular spectrum of the second-harmonic intensity are correlated with angular positions of the split CMC modes and caused by combination of the resonant enhancement of the fundamental radiation and constructive interference of the second-harmonic fields induced in the microcavity spacers. The shape of the SHG resonances is shown to be dependent on the variation of the electromagnetic coupling between the microcavities controlled by reflectivity of the intermediate distributed Bragg reflector.

DOI: 10.1103/PhysRevB.68.233303 PACS number(s): 78.67.−n, 42.65.Ky, 42.70.Qs

Nonlinear optics of photonic crystals and photonic-crystal microcavities[1,2] stands out as one of the prospective areas of modern optics. Microcavity is a photonic crystal with one of the unit cells replaced by the unit cell with different optical parameters. In one-dimensional case, photonic-crystal microcavities can be obtained, for instance, if spacer with the optical thickness of $\lambda_0/2$ for certain wavelength λ_0 is incorporated into photonic crystal formed from $\lambda_0/4$-thick layers with alternating refractive indices. It brings to appearance the microcavity mode in the photonic band gap (PBG) centered at λ_0 at the normal incidence. The optical wave is localized in the spacer in case of the wavelength-angular resonance with the microcavity eigenmode, i.e., as $k_\parallel d_{MC}=\pi$, where $k_\parallel$ is the component of the wave vector in the d_{MC}-thick microcavity spacer parallel to the periodicity direction. Coupled microcavities[3] (CMC) are formed from the photonic crystal with several spacers. The coupling between localized modes of CMC leads to formation of photonic defect band within the PBG.[4,5] Due to this waveguiding band, full transmission of light can be observed inside PBG.[6] One-dimensional photonic crystal with two identical spacers is the simplest structure of CMC. Such coupled microcavities have two eigenmodes, which are symmetric and antisymmetric ones: the electromagnetic field has either the same or π-shifted phases in the spacer centers [Figs. 1(a) and 1(b)]. Transmission or reflection spectra have two resonance features in PBG, which are split spectrally because of the electromagnetic coupling between microcavities.[7] The coupling is defined by transmittance of intermediate photonic crystal. CMC open up new approaches to control the light-matter interaction in solids. For example, resonance coupling between exciton states of quantum wells embedded in the CMC with the photon eigenmode of CMC leads to formation of cavity polaritons.[8] The fascinating effects found recently in CMC include dual lasing under optical pumping,[9] increasing of Rabi splitting for photon-exciton (polariton) modes,[10] and asymmetric photoluminescence emission.[11] The amplitude of the optical wave resonant to one of the CMC modes increases strongly in the spacers that should lead to the resonant enhancement of the nonlinear-optical response, such as second-harmonic generation (SHG). However, SHG has not been observed in CMC up to now, although strong manifestation of the optical coupling between spacers is expected in the SHG response.

Mesoporous silicon is a promising material for PBG structure fabrication. Photonic crystals formed from mesoporous silicon are made by the electrochemical etching of silicon by means of periodic variation of chemical reaction parameters during the etching process.[12] The strong spatial localization of the resonant optical field in porous silicon microcavities, directly probed by near-field optical scanning microscopy,[13] results in narrowing and tuning of photoluminiscence,[14] the manyfold enhancement of Raman scattering,[15] and giant second-[13] and third-harmonic[16] generations. The high-quality-factor CMC can be fabricated from mesoporous silicon as it has been demonstrated recently for two-spacer[17] and multiple-spacers[18] CMC.

In this paper, intensity enhancement of SHG in CMC upon the fundamental wave resonance with the split CMC modes is studied. The angular spectra of the second-harmonic (SH) intensity measured on the series of the CMC samples formed from mesoporous silicon with varied reflectivity of the intermediate Bragg reflector show the strong dependence on the electromagnetic coupling between two identical spacers.

CMC are fabricated by the electrochemical etching of the optically polished p^+-type Si(001) wafers with resistivity of 0.005Ω cm in electrolyte containing 15% of fluoric acid, 27% of water, and 58% of ethanol. After chemical removal of the native oxide, the silicon wafer is set into the electrochemical cell and tightly clamped by its backside to a flat copper cathode. The platinum spiral anode is immersed into electrolyte. The density of the current, flowing through the wafer, defines the porosity of the etching porous silicon layer. The layer thickness is controlled by etching time. Since the silicon etching process is self-limited and the porous silicon layer once etched is excluded from the subsequent etching,[12] the profile of ''current density/time'' transforms into the profile of ''porosity (refractive index)/thickness.'' The CMC samples consist of three photonic crystals, separated by two identical $\lambda_0/2$-thick spacers with corresponding wavelength of $\lambda_0 \simeq 1200$ nm [inset in Fig. 1(c)]. External Bragg reflectors are formed from four pairs of

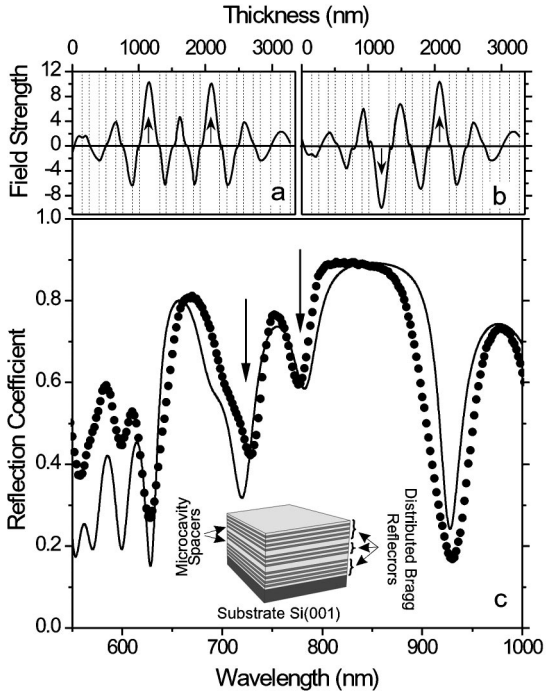

FIG. 1. (a) and (b) Spatial distribution across porous silicon CMC of the field strength of the optical wave resonant with short-wavelength [panel (a)] and long-wavelength [panel (b)] CMC modes. The incident wave amplitude is equal to unit. Dash lines indicate the interfaces between porous silicon layers. Arrows emphasize the field phases in the spacer centers. (c) The reflection spectrum of the porous silicon CMC with $\lambda_0 \simeq 800$ nm and $N=5$ measured for 45° angle of incidence of *s*-polarized wave. Curve is the fit to the data by the transfer-matrix formalism. Arrows indicate the eigenmodes positions. The inset: sketch of the sample.

λ_0/4-thick layers of porous silicon. The number of layers in the intermediate Bragg reflector (IBR), N, is changed in series from three to nine. Porous silicon layers with the high refractive index are etched with the current density of 25 mA/cm^2 during 7.2 sec, the layers with the low refractive index are formed during the 3.6 sec-etching with the current density of 83 mA/cm^2. The refractive indices of the porous silicon layers are found from the calibration reflection spectra of the single porous silicon layers. Porosities of layers are calculated using effective medium approximation.[12] Layers with the high refractive index have $n_H=1.78$ and porosity of $f_H=0.64$, and layers with the low refractive index have $n_L=1.42$ and $f_L=0.77$. The refractive index of spacers is n_L. The CMC with $N=5$ and the same refraction indices but with λ_0 shifted to 800 nm is fabricated for linear reflection spectroscopy in the wavelength domain, since angular spectroscopy allows tuning in the narrow region covering only vicinity of the modes of the CMC samples with $\lambda_0 \simeq 1200$ nm.

Wave-vector domain SHG spectroscopy is performed by tuning the angle of incidence θ of the *s*-polarized output of the 10 ns-YAG:Nd^{3+} laser at wavelength of 1064 nm with energy of ≈10 mJ per pulse and spot diameter of 1 mm. The goniometer provides the rotation of the sample and detection system in the range of angle of incidence from 15° to 80°.

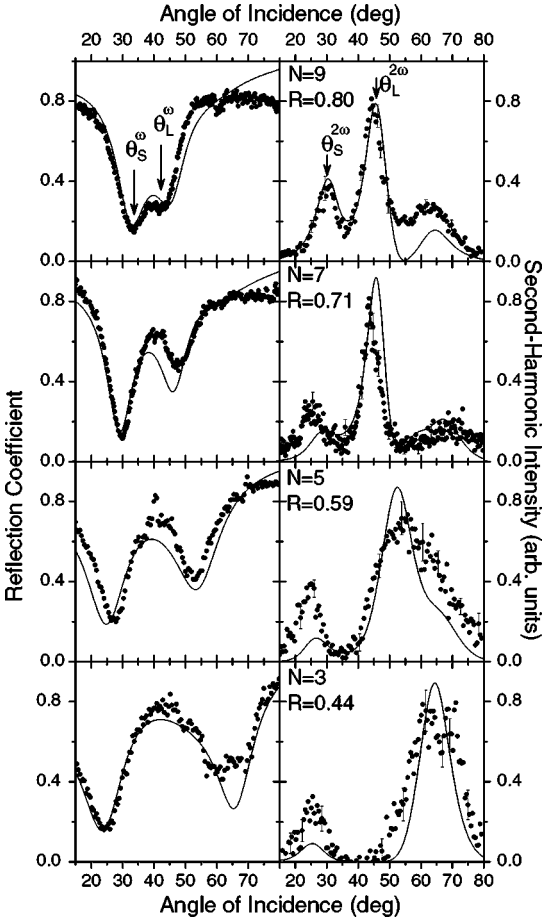

FIG. 2. Angular spectra of SH intensity (right panels) and linear reflection coefficient (left panels) of porous silicon CMC with $\lambda_0 \simeq 1200$ nm and different reflection coefficient of IBR, R. Lines are the fit results by the transfer-matrix formalism. $\theta_S^{\omega(2\omega)}$ and $\theta_L^{\omega(2\omega)}$ denote angular positions of resonance features in linear and SHG spectra, corresponding to the short- and long-wavelength modes of CMC, respectively.

The radiation reflected from the CMC sample passes through color and interference filters extracting the SH light and a Glan prism separating the *p*-polarized SH wave. The SHG signal is detected by a photomultiplier tube and a gated electronics. The angular spectrum of the linear reflection coefficient is measured in the identical alignment.

The linear reflection spectrum of the porous silicon CMC measured in the wavelength domain is shown in Fig. 1(c). The spectrum has a plateau with high reflectivity, corresponding to the PBG, and two resonant dips at ≈730 and 780 nm. These drops of the reflection coefficient correspond to the split CMC modes, since the fundamental radiation resonant with the CMC eigenmodes propagates efficiently in CMC and is localized into and in the vicinity of spacers, as it is shown in Figs. 1(a) and 1(b).

Figure 2 shows the angular spectra of the fundamental wave reflection and the SH intensity measured at the series of porous silicon CMC with different reflectivity of the intermediate Bragg reflector. The linear spectra have two dips, where reflection coefficient value decreases up to 0.2, corresponding to the resonance of the fundamental radiation with

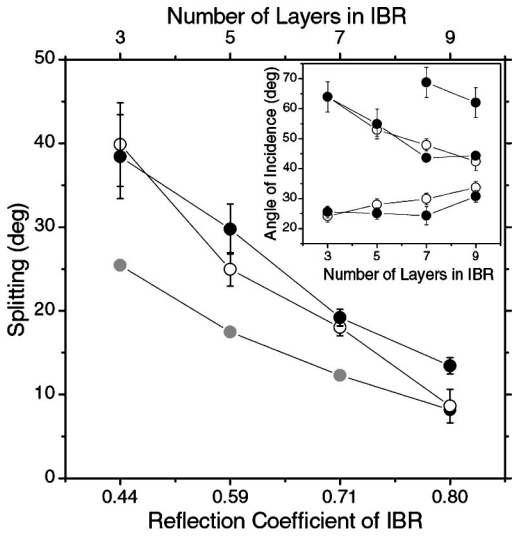

FIG. 3. Dependences of the angular splitting of the SHG resonances, $\theta_L^{2\omega}-\theta_S^{2\omega}$, (filled circles) and the linear reflection coefficient dips, $\theta_L^{\omega}-\theta_S^{\omega}$, (open circles) on the number of layers in the intermediate Bragg reflector and its reflection coefficient. Gray circles show the model dependence of the splitting of the linear reflection coefficient dips for the ideal CMC. Inset: the angular positions of SHG and linear reflection resonances.

the CMC modes. In the other parts of spectra, reflection coefficient reaches the values up to 0.85 that corresponds to the PBG. For all CMC samples, the right dip in the spectra related to the long-wavelength mode of CMC is shallower than the left one that can be attributed to the monotonous decrease of optical thickness of porous silicon layers with the depth.[19]

Angular spectra of the SH intensity have resonant features in the range of θ from 20° to 70°. Angular positions of the SHG peaks at $\theta_S^{2\omega}$ and $\theta_L^{2\omega}$ correlate with the CMC mode positions defined from the reflection spectra of fundamental radiation. However, they are slightly shifted from positions of the dips of linear reflection coefficient and located mostly on their external slopes. The SH intensity increases up to two orders of magnitude in comparison with the SHG signal in the PBG. For all CMC samples, the amplitude of the SHG peak at $\theta_L^{2\omega}$ exceeds the SHG enhancement in the peak at $\theta_S^{2\omega}$. The full width at half maximum of the long-wavelength peaks increases with R decrease from $\approx 9°$ for CMC with $N=9$ to 16° for the sample with $N=3$. Additional buildup of the SH intensity at $\approx 65°$ is observed in the SHG spectra of the CMC samples with $N=7$ and $N=9$. The angular splitting of dips in reflection spectra and SHG peaks as a function of the thickness of the intermediate Bragg reflector is shown in Fig. 3. It decreases gradually with the increase of the IBR reflectivity that characterizes the reduction of the coupling between microcavities.

The observed SHG enhancement is caused by the increase of the amplitude of the resonant fundamental field inside CMC. The spatial distributions of the field strength along the periodicity direction z are shown in Figs. 1(a) and 1(b). They are calculated for CMC with $N=5$ by using transfer-matrix formalism with the plane $z=0$ corresponding to the CMC-air interface. The fundamental field amplitude in the spacer centers is approximately tenfold enhanced in comparison with that of the incident wave. Since fundamental field localization inside the microcavity spacers is maximal at the resonance with the CMC modes, the angular positions of the SHG peaks are located near the dips of the linear reflection spectra. The fundamental field is enhanced both in spacers and in surrounding layers of Bragg reflectors, and the nonlinear sources contributed to SHG are extended over the micron-size distance. Thus the magnitude and shape of the SHG peaks are influent significantly by interference of the partial contributions to the total outgoing SH field from various layers of CMC. The phases of these partial SH fields, calculated within the nonlinear transfer-matrix formalism,[20] depend essentially on the spectral position of CMC modes governed by refractive indices and thicknesses of porous silicon layers. It is shown that destructive interference of the SHG partial contributions results in the splitting of the SHG peaks at the long-wavelength mode for the sample with $N=7$ and $N=9$ and in the changes of their amplitudes. Interference effects define also the spectral shift of the SHG resonances from the dip minima of the linear reflection spectra.

SHG spectra are fitted within the nonlinear transfer-matrix formalism. The effective dipole quadratic susceptibility of mesoporous silicon layers in CMC, $\chi^{(2),j}$, arisen due to the inversion symmetry breaking at the pore walls, is supposed to be constant inside each jth layer[13] and depends on porosity proportionally to $1-f_j$. The $\chi^{(2)}$ contributions from opposite pore walls do not interfere destructively anymore, as it was in microporous silicon, since the pore size in mesoporous silicon is in the order of several tens of nanometers. Macroscopically, this leads to the $\chi_{zxx}^{(2),j}=\chi_{zyy}^{(2),j}$ nonzero elements of $\chi^{(2),j}$ for the s-in, p-out polarization combination related to the medium, which is isotropic in the xy plane. The model spectra of reflection coefficient and the SH intensity are calculated for ideal CMC structure, in which optical thicknesses of layers of Bragg reflectors are equal to $\lambda_0/4$ exactly and layer thicknesses are taken to be $D_H^{\lambda/4}=212$ nm, and $D_L^{\lambda/4}=169$ nm for $\lambda_0=1200$ nm. The curves fit well the SHG resonances and drops in the linear spectra, but demonstrate the higher quality factors of resonances and the smaller splitting values, that is shown in Fig. 3. It indicates that the Bragg reflectors in the real CMC have smaller reflectivity than expected one. The better agreement with the data is achieved if the corrections accounting for the increase of porosity and reduction of refraction index of porous silicon layers with the depth are taken.[18] The porosity modulation is caused by the inhomogeneity of the etching process with the depth and the gradual porous silicon oxidation[19] inside the CMC samples. Curves in Fig. 2 show the results of the simultaneous fit of the spectra achieved with the same parameters for all CMC samples. The best agreement with the data is obtained with the parabolic modulation of the porosity. Porosity of the jth layer is taken as $f_j=f_{0,j}+A[1-((K-j)/K)^2]$, where $f_{0,j}$ is the initial porosity, K is the total number of layers, and A is the maximal porosity modulation. The maximal deviation of refractive index of the deepest layer from ideal model does not exceed 0.05. A similar result is achieved by reduction of the layer thickness with

the depth: the deeper layers have smaller thickness than layers near the surface of the sample. The fit of the experimental spectra with the small parabolic deviation of parameters of CMC samples with the depth can be used for updating a technique of preparation of photonic crystals and microcavities based in porous silicon.

In conclusion, the enhancement of second-harmonic generation in the coupled microcavities based on the all-silicon photonic crystals is studied. The SH intensity enhancement is observed at the resonance of the fundamental radiation with the CMC eigenmodes. Angular splitting of the peaks in the SH intensity spectra shows monotonous dependence on magnitude of coupling between two identical microcavity spacers controlled by the reflectivity of the intermediate Bragg reflector. The basic mechanism of the SHG enhancement is localization of the fundamental field in the spacers, which leads to the increase of the amplitudes of the SH fields induced inside them. Constructive interference of the outgoing SH fields from the various layers of CMC results in the redistribution of amplitudes of SHG resonances and the shift of peaks from angular positions corresponding to the maximal localization of the fundamental field.

This work was supported by the Presidential Grant for Leading Russian Science Schools and the Russian Foundation for Basic Research.

---

*URL: http://www.shg.ru

[1] J. Joannopoulos, R. Meade, and J. Winn, *Photonic Crystals: Molding the Flow of Light* (Princeton University, Princeton, NJ, 1995).

[2] K. Sakoda, *Optical Properties of Photonic Crystals* (Springer, Berlin, 2001).

[3] R.P. Stanley, R. Houdre, U. Oesterle, M. Ilegems, and C. Weisbuch, Appl. Phys. Lett. **65**, 2093 (1994).

[4] N. Stefanou and A. Modinos, Phys. Rev. B **57**, 12 127 (1998).

[5] A. Yariv, Y. Xu, R.K. Lee, and A. Scherer, Opt. Lett. **24**, 711 (1999).

[6] M. Bayindir, S. Tanriseven, and E. Ozbay, Appl. Phys. A: Mater. Sci. Process. **A72**, 117 (2001).

[7] M. Bayindir, C. Kural, and E. Ozbay, J. Opt. A, Pure Appl. Opt. **3**, 184 (2001).

[8] R. Houdre, C. Weisbuch, R.P. Stanley, U. Oesterle, P. Pellandini, and M. Ilegems, Phys. Rev. Lett. **73**, 2043 (1994).

[9] P. Pellandini, R.P. Stanley, R. Houdre, U. Oesterle, M. Ilegems, and C. Weisbuch, Appl. Phys. Lett. **71**, 864 (1997).

[10] A. Armitage, M.S. Skolnick, V.N. Astratov, D.M. Whittaker, G. Panzarini, L.C. Andreani, T.A. Fischer, J.S. Roberts, A.V. Kavokin, M.A. Kaliteevski, and M.R. Vladimirova, Phys. Rev. B **57**, 14 877 (1998).

[11] M. Emam-Ismail, V.N. Astratov, M.S. Skolnick, D.M. Whittaker, and J.S. Roberts, Phys. Rev. B **62**, 1552 (2000).

[12] O. Bisi, S. Ossicini, and L. Pavesi, Surf. Sci. Rep. **38**, 1 (2000).

[13] T.V. Dolgova, A.I. Maidykovski, M.G. Martemyanov, A.A. Fedyanin, O.A. Aktsipetrov, G. Marowsky, V.A. Yakovlev, and G. Mattei, Appl. Phys. Lett. **81**, 2725 (2002).

[14] V. Pellegrini, A. Tredicucci, C. Mazzoleni, and L. Pavesi, Phys. Rev. B **52**, R14 328 (1995).

[15] L.A. Kuzik, V.A. Yakovlev, and G. Mattei, Appl. Phys. Lett. **75**, 1830 (1999).

[16] T.V. Dolgova, A.I. Maidykovski, M.G. Martemyanov, A.A. Fedyanin, and O.A. Aktsipetrov, Pis'ma Zh. Eksp. Teor. Fiz. **75**, 17 (2002) [JETP Lett. **75**, 15 (2002)].

[17] L. Pavesi, G. Panzarini, and L.C. Andreani, Phys. Rev. B **58**, 15 794 (1998).

[18] M. Ghulinyan, C.J. Oton, Z. Gaburro, P. Bettotti, and L. Pavesi, Appl. Phys. Lett. **82**, 1550 (2003).

[19] A.G. Cullis, L.T. Canham, and P.D.J. Calcott, J. Appl. Phys. **82**, 909 (1997).

[20] D.S. Bethune, J. Opt. Soc. Am. B **6**, 910 (1989).